

## Article

# Mountain Streambed Roughness and Flood Extent Estimation from Imagery Using the Segment Anything Model (SAM)

Beata Baziak <sup>1,\*</sup> , Marek Bodziony <sup>1</sup>  and Robert Szczepanek <sup>2</sup> 

<sup>1</sup> Department of Geoengineering and Water Management, Faculty of Environmental and Energy Engineering, Cracow University of Technology, 31-155 Krakow, Poland; marek.bodziony@pk.edu.pl

<sup>2</sup> Institute of Geological Sciences, Faculty of Geography and Geology, Jagiellonian University, 30-387 Krakow, Poland; robert.szczepanek@uj.edu.pl

\* Correspondence: beata.baziak@pk.edu.pl

**Abstract:** Machine learning models facilitate the search for non-linear relationships when modeling hydrological processes, but they are equally effective for automation at the data preparation stage. The tasks for which automation was analyzed consisted of estimating changes in the roughness coefficient of a mountain streambed and the extent of floods from images. The Segment Anything Model (SAM) developed in 2023 by Meta was used for this purpose. Images from many years from the Wielka Puszca mountain stream located in the Polish Carpathians were used as the only input data. The model was not additionally trained for the described tasks. The SAM can be run in several modes, but the two most appropriate were used in this study. The first one is available in the form of a web application, while the second one is available in the form of a Jupyter notebook run in the Google Colab environment. Both methods do not require specialized knowledge and can be used by virtually any hydrologist. In the roughness estimation task, the average Intersection over Union (IoU) ranges from 0.55 for grass to 0.82 for shrubs/trees. Ultimately, it was possible to estimate the roughness coefficient of the mountain streambed between 0.027 and 0.059 based solely on image data. In the task of estimation of the flood extent, when selecting appropriate images, one can expect IoU at the level of at least 0.94, which seems to be an excellent result considering that the SAM is a general-purpose segmentation model. It can therefore be concluded that the SAM can be a useful tool for a hydrologist.

**Keywords:** hydrology; flood; image segmentation; machine learning; computer vision; manning roughness coefficient



**Citation:** Baziak, B.; Bodziony, M.; Szczepanek, R. Mountain Streambed Roughness and Flood Extent Estimation from Imagery Using the Segment Anything Model (SAM). *Hydrology* **2024**, *11*, 17. <https://doi.org/10.3390/hydrology11020017>

Academic Editor: Alessio Radice

Received: 15 December 2023

Revised: 25 January 2024

Accepted: 26 January 2024

Published: 31 January 2024



**Copyright:** © 2024 by the authors. Licensee MDPI, Basel, Switzerland. This article is an open access article distributed under the terms and conditions of the Creative Commons Attribution (CC BY) license (<https://creativecommons.org/licenses/by/4.0/>).

## 1. Introduction

Observing hydrological phenomena occurring in the natural environment is not an easy task, especially in hard-to-reach areas. Maintaining a monitoring network is expensive, which is why the number of traditional measurement stations decreases every year. However, there is a growing interest in using alternative sources of information, such as satellite images or images from surveillance cameras. This became possible mainly thanks to the rapid development in recent years of machine learning systems, which can automatically extract a lot of valuable information from such materials. This type of model is increasingly used in hydrology, e.g., to monitor the water level in rivers [1,2], flood monitoring [3,4] or determining flood zones [5] Pally and Samadi [6] used R-CNN, YOLOv3 and Fast R-CNN for flood image classification and semantic segmentation. Erfani et al. [7] developed ATLANTIS, a benchmark for semantic segmentation of waterbody images.

The main directions of hydrological research are directly related to process and time series modeling, but machine learning is increasingly used in data pre-processing [8].

One of the important elements influencing the water flow in the river is the riverbed roughness coefficient. It is related to the resistance due to friction acting along the perimeter

of the wetted trough and the resistance created by objects directly washed by the water. Large objects such as stones, boulders, bushes, trees and logs significantly increase the bed roughness factor. When larger flows occur, they may cause water damming and pose a flood risk [9–11]. This is why a good estimate of roughness has a significant impact on the results of hydrological models. However, in catchments with high flow dynamics, for example mountain ones, this parameter changes rapidly due to the material carried away by the floods and the vegetation developing intensively within the riverbeds. Tracking these changes using traditional methods would require frequent measurements and would be extremely expensive. One alternative to collecting and updating such data may be the use of various types of images. Computer vision was so far used by scientists mainly to estimate the height of the water table [12]. However, modern computer vision systems make it possible to obtain semantic information from such data; for example, about the type of land cover. In addition to dedicated segmentation systems, such as state-of-the-art panoptic segmentation [13], general-purpose segmentation systems are gaining popularity. One of the newest general models with zero-shot transfer capability is the Segment Anything Model (SAM) released by Meta in April 2023 [14].

Thanks to its general-purpose structure and training data, the SAM can be used for many tasks. In medical imaging, the SAM can be used to segment different structures and tissues in images, such as tumors, blood vessels and organs [15,16]. This information can be used to assist doctors in diagnosis and treatment planning. So far, most publications exploiting the possibility of using the SAM for image segmentation have appeared in the field of medicine. In agriculture, the SAM can be used to monitor crop health and growth. By segmenting different areas of a field or crop, the SAM can identify areas that require attention, such as areas of pest infestation or nutrient deficiency [17]. In earth sciences, the SAM has been used for superglacial lake mapping [18], but for the task of flood inundation mapping we only managed to find information about the possible potential use of the SAM [19]. This is therefore an area of applicability of the model to potentially explore.

The goal of the SAM is automatic promptable segmentation with minimal human intervention. It is a deep learning model, trained on the SA-1B dataset, the largest segmentation dataset to date—over one billion masks spread across 11 million carefully curated images [14]. The model has been trained to achieve outstanding zero-shot performance, surpassing previous fully supervised results in numerous cases. Zero-shot transfer refers to the SAM's ability to adapt to new tasks and object categories without requiring explicit training or prior exposure to specific examples [20]. The model predicts object masks only and does not generate labels. The SAM was trained to return segmentation masks for any prompt understood as point, bounding box, text or any other information indicating what to segment on an image. An alternative method is the automatic segmentation of an image as a whole using a grid of points. In this case, the SAM tries to segment any object on the image. The SAM is available as source code in the public repository and as a web application (<https://segment-anything.com/demo#>; accessed on 20 January 2024), giving the opportunity to test its capabilities without the need for coding. Therefore, each user can choose a version of the model appropriate to his or her experience with machine learning models. One such potential user group may be hydrologists, and it is from their perspective that we tried to analyze the possibilities of using the SAM.

The aim of this study is to use the Segment Anything Model in hydrology to determine changes in the roughness of a mountain riverbed based on images in various vegetation periods over the years 2010–2023. The second goal is to estimate the extent of water in the streambed based on the same images. The results can be used to quickly determine flood zones in the event of floods.

## 2. Materials and Methods

This study focuses on a simple and automatic solution that allows obtaining data that can be used in hydrological modeling. From a modeling perspective, the type of coverage in the riverbed area is particularly important. In the case of mountain catchments covered

with forest, obtaining this type of data is difficult when using only orthophotomaps and aerial photos. The best solution is field measurements or the use of local monitoring. Unfortunately, manual methods are time-consuming and expensive. Therefore, there is a need to use tools and methods that allow automatic or semi-automatic analysis using other data sources, e.g., photographic documentation or local video monitoring.

### 2.1. Study Area

The study area is the Wielka Puszcza river catchment (Great Forest in Polish) located in the southern part of Poland, in the Beskid Mały Mountains. The stream is a right-bank tributary of the Soła River, which is a right-bank tributary of the Vistula, the largest river in the country. The mouth of the Wielka Puszcza stream is located in the backwater of the dam reservoir located in the town of Czaniec (Figure 1). The Wielka Puszcza is a mountain catchment area characterized by steep slopes, impermeable soil and a dense river network. About 90% of the catchment area is forest, 7% is agricultural land and 3% is built-up area. The physiographic parameters of the catchment are presented in Table 1.

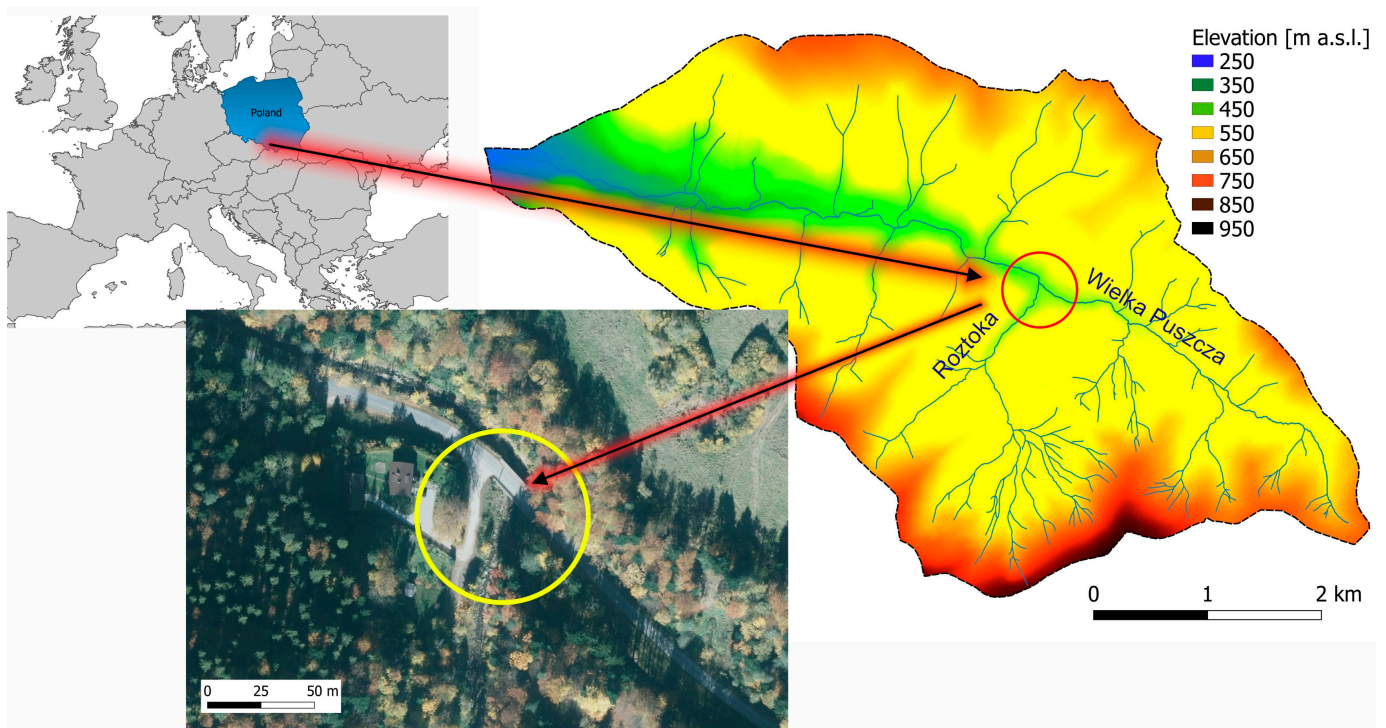


**Figure 1.** The Wielka Puszcza river catchment and location of the analyzed research cross-section (source DEM and orthophotomap: [mapy.geoportal.gov.pl](https://mapy.geoportal.gov.pl); accessed on 20 January 2024).

**Table 1.** Physiographic parameters of the Wielka Puszcza river catchment.

Parameter	Value
Catchment area	20.05 [km <sup>2</sup> ]
Main watercourse length	9.44 [km]
Watercourse slope	43.75 [‰]
River source elevation	710 [m a.s.l.]
Estuary elevation	297 [m a.s.l.]

The Wielka Puszcza stream has been a research catchment area of the Cracow University of Technology since the 1970s. In the 1990s, meteorological observations were carried out at seven measurement stations. Additionally, measurements of water levels and flows in one cross-section were also carried out. In 2005, as a result of catastrophic rainfall and flooding, the measuring station was destroyed, which resulted in its liquidation (Figure 2).

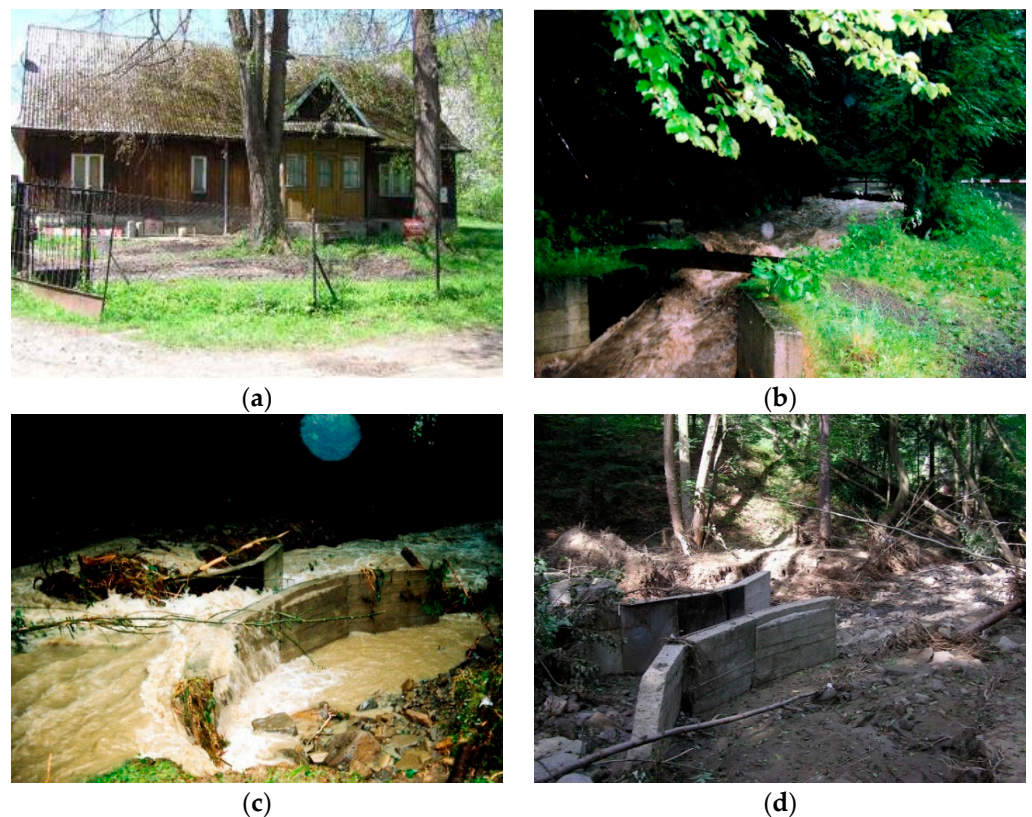


**Figure 2.** The Wielka Puszcza—research station of the Cracow University of Technology in 1993–2005, (a) lodge; (b) measuring cross-section before the flood; (c) measuring cross-section during the flood; (d) measuring cross-section after the flood.

In 2017, hydrological measurements resumed on a limited basis at a new location. Currently, observations of water levels using a radar sensor are being carried out, as well as visual monitoring of the water table level, in the form of images taken by an industrial camera operating in visible light and infrared (day and night). Two Hellmann's trough rain gauges are also installed, providing an automatic system for measuring precipitation height every 10 min (Figure 3). The data are collected in the recorder and sent to a server located at the Cracow University of Technology, which makes it possible to conduct online observations of the water table level in the stream and the precipitation.

## 2.2. Data

The analyzed area is a mountainous catchment with no continuous measurement system. The only publicly available data sources are orthophotos and satellite images. In the considered period 2010–2023, the orthophoto update took place only in year 2010 and 2023. Unfortunately, due to the nature of the terrain covered by dense forest, orthophotomaps, even in high resolution, are not suitable for assessing changes in the riverbed. For this reason, terrestrial photographs were used to determine the type of coverage in the streambed. Photographs do not allow results to be obtained as accurately as when using an orthophotomap, but by using characteristic points in the cross-section, it is possible to map the geometry of the riverbed even in photos taken from ground level. In the case of forested catchments, this is practically the only method. The data for the Segment Anything Model consist of photographic documentation by Marek Bodziony taken in the catchment area, at the junction of the Wielka Puszcza and Roztoka streams. Seven photos showing the riverbed in the selected cross-section were used for analysis. The photos are from three growing seasons: spring in the years 2010, 2011 and 2023, autumn in the years 2011, 2015 and 2023 and winter in 2012 (Figure 4). Photographic documentation is available on

the website [https://holmes.iigw.pl/~mbodzion/zaklad/wielka\\_puszcza/](https://holmes.iigw.pl/~mbodzion/zaklad/wielka_puszcza/) (accessed on 20 January 2024).

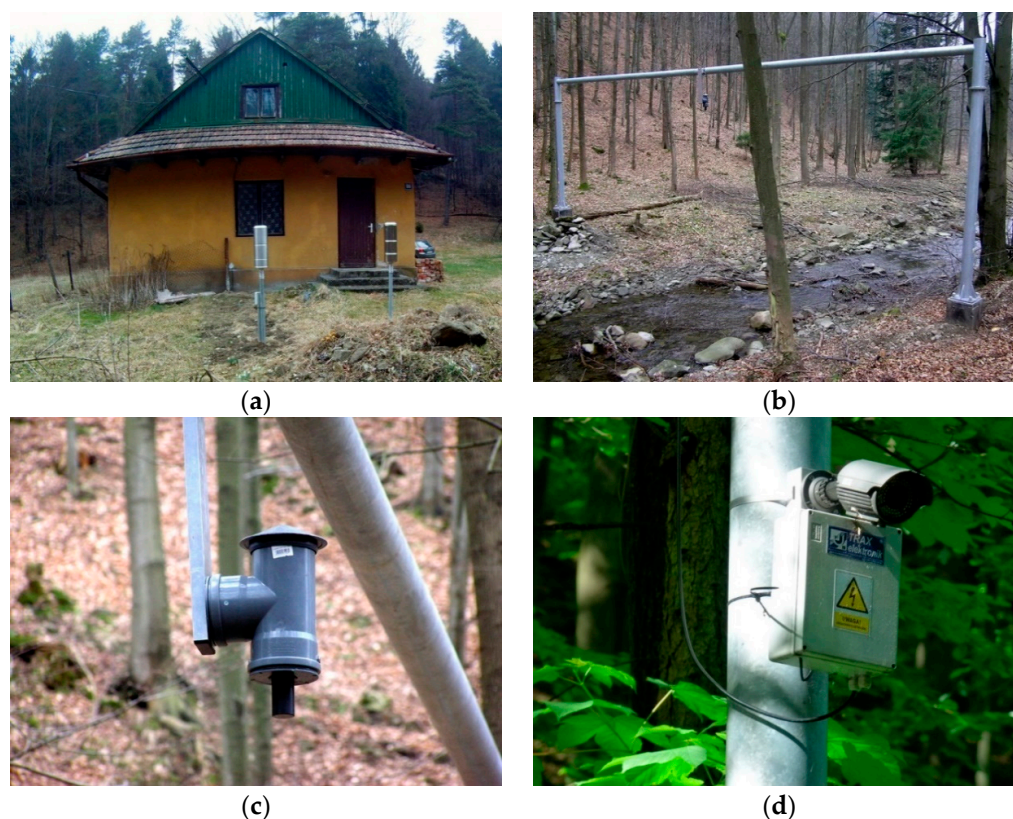


**Figure 3.** The Wielka Puszcza—Cracow University of Technology’s new research station operating since 2017, (a) measuring rainfall with Hellman rain gauges; (b) water table level monitoring; (c) water table level measurement sensor; (d) camera taking pictures of the water table level.

### 2.3. Methods

The presented workflow is divided into two parts using identical data and tools, but for different purposes. The basis for the analysis is photos showing the valley of a mountain stream at the junction of two watercourses.

The aim of the first part of the analysis was to estimate the roughness of the riverbed based on the segmentation results. The water category was omitted in this analysis. The aim of the second part was to assess to what extent the presented model can be used to estimate the extent of floods. Only the water category was used in this analysis.

For ungauged catchments where the flow is not measured, the roughness coefficient cannot be optimized. An alternative solution is to adopt an average roughness coefficient for sections with a similar type of coverage. The proposed method involves determining a cross-section based on the Digital Elevation Model (DEM) divided into sections with a similar type of coverage (Figure 5b). Because the photos were taken from known locations, it was possible to geometrically convert characteristic points from the photos into points from the orthophotomap. In this way, photo units (px) were converted to map units (m), enabling the calculation of the roughness coefficient in the entire examined cross-section. For each section (zone) shown in Figure 5, the average roughness coefficient was calculated by analyzing the type of coverage 3 m upstream and downstream from the central A-A cross-section. Identification of the type of coverage based on photographs with the SAM model was used to estimate the weighted average roughness coefficient for the given cross-section. Based on the determined roughness coefficient, the flow in the stream can be estimated using Manning’s formula. Assuming steadyflow and one-dimensional

schematization, the cross-sectional geometry and slope of the stream determined from the DEM can be used for calculations.



**Figure 4.** Photographs of different vegetation periods in the considered years 2010–2023.

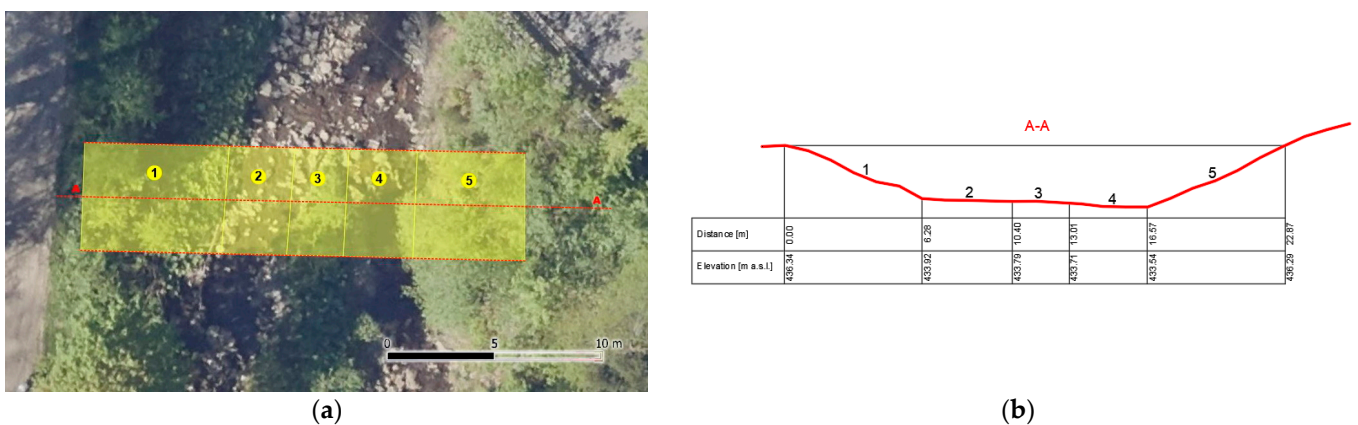


**Figure 5.** Sample cross-section for roughness coefficient estimation: (a) division into sections of the wetted perimeter with different roughness coefficients, (b) cross-section based on DEM (source: DEM and orthophotomap from [maps.geoportal.gov.pl](https://maps.geoportal.gov.pl); accessed on 20 January 2024).

We estimate the initial Manning’s roughness coefficient  $n_0$  through the observation of the river channel coverage. This method is also documented by other authors [21]. However, none of the methods we found used computer vision or machine learning to automate this process. There are only works that use satellite images to estimate coefficient

n through LULC classification [22,23]. Usually, the last step in determining n is its optimization using available hydrological data which are, however, unavailable in the case of uncontrolled catchments.

Using the SAM automatic segmentation model, objects in photos are recognized, but without assigning labels to them. The labeling process was performed non-automatically by assigning designated segments to one of the categories specified in Table 2. The segmentation analysis was limited in each case to the area defined as the streambed.

**Table 2.** Object categories within riverbed used in this study with corresponding Manning’s roughness coefficient (according to Chow [24]).

Category	Manning’s Roughness Coefficient n
Stones	0.040
Earth channel	0.025
Grass	0.030
Shrubs/tree	0.100

To determine the index related to the roughness of the riverbed ( $R_c$ ), the relationship between Manning’s roughness coefficient ( $n$ ) and the area of coverage for each of the adopted coverage categories was assumed:

$$R_c = \frac{\sum_{i=1}^m n \cdot A_C}{\sum_{i=1}^m A_C} \quad (1)$$

where:

$R_c$ —riverbed roughness index [ $m^{-1/3} s$ ];

$n$ —Manning’s roughness coefficient for category [ $m^{-1/3} s$ ];

$A_C$ —coverage area for the category [ $px$ ].

The SAM supports three main segmentation modes in the online version: fully automatic mode, bounding box mode and point mode. This study tested the first two modes. In addition, automatic segmentation was performed using the Google Colaboratory (Colab) environment using the Jupyter notebook provided by the SAM authors. Both versions are based on the same SAM, but only one of them (SAM Colab) offers the possibility of changing model parameters through scripts.

**SAM ONLINE:** The fully automatic segmentation mode involves generating masks automatically based on a regular grid of points. An example of using this mode on a selected image is shown in Figure 6a.

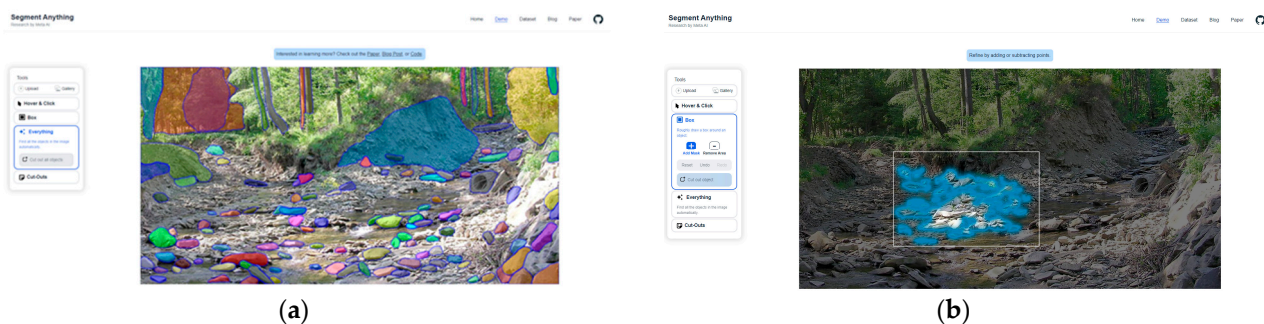


**Figure 6.** User interface of two SAM online modes (a) automatic, (b) bounding box.

**BOUNDING BOX ONLINE:** To segment only a specific portion of an image, the bounding box mode can be used. An example of using this mode on a selected image is shown in Figure 6b.

Image segmentation using the bounding box method requires manual selection of the objects. Its use is therefore not the best solution for automatically generating areas of land cover type in a watercourse area. Due to the necessity of pointing out objects each time, this method is time-consuming and unsuited to the needs of the presented analysis. Tests verifying the segmentation of water-covered areas showed its low efficiency, so already at the test stage this method was abandoned for analysis.

SAM COLAB: Google Colaboratory (Colab) is a public service for running Jupyter notebooks directly in the browser without configuration (Figure 7). It provides free GPU access and facilitates code sharing. Using the sample Jupyter notebook provided in the project repository, image segmentation was performed. It should be mentioned that model parameters were not modified or tuned for this analysis. The results obtained in this way will therefore be suboptimal, but for the purposes of these tests it is assumed that the user of the tools is a hydrologist without in-depth knowledge of machine learning methods and optimization of these models. As a result of image segmentation, a segmentation mask is created, as well as a file containing the identifiers and geometry of the masks.

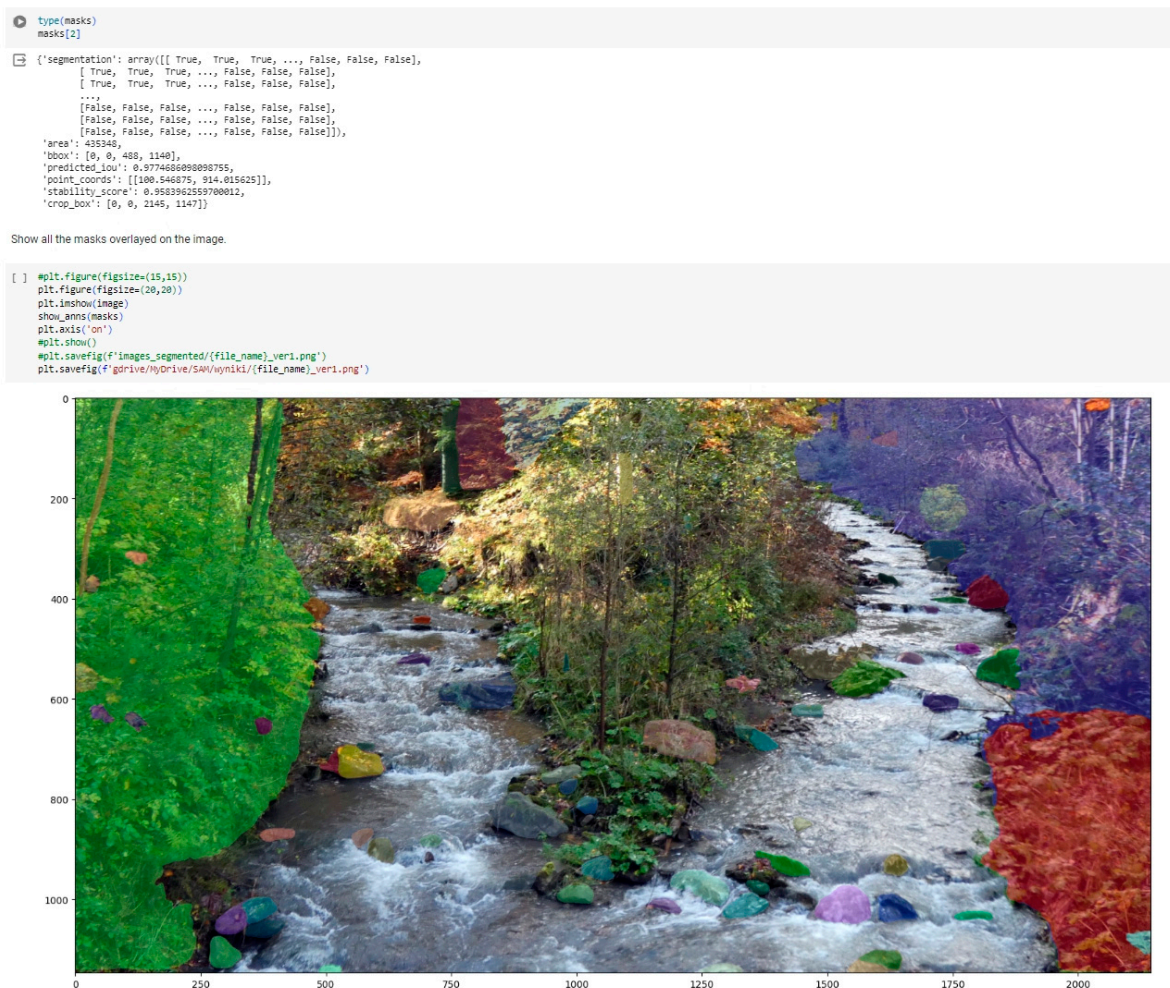


**Figure 7.** Image segmentation in Jupyter notebook on Google Colaboratory (Colab).

SAM online is a web-based version that can be used by inexperienced users. SAM Colab should be used by hydrologists with programming experience; however, in the presented study we used default model parameters. Unfortunately, based on the available literature, we were unable to determine what parameters were adopted for SAM online. Our analyses show that the SAM was trained for segmentation on physical objects with precisely defined area boundaries (objects). In the case of complex images with ambigu-

ous object boundaries, such as forest areas, streams, etc., the segmentation results may require user intervention in the model parameters. In the case of SAM Colab, a large number of parameters to optimize requires additional research and is beyond the scope of this manuscript.

Four categories were adopted to identify the type of cover of the riverbed area, which have a decisive influence on the riverbed roughness parameter: earth channel, stones, grass and shrubs/trees. The earth channel category includes areas consisting of small stones and gravel constituting a uniform surface. Objects distinguished by their size and shape from the earth channel area were classified as stones. Grass is an area covered with low grassy vegetation. Areas of medium and tall vegetation were included in the shrubs/trees category. Image analysis in the SAM was carried out based on the segmentation of adopted categories, the areas of which were defined in image units (pixels), not in physical units. Areas for which the SAM did not assign a mask most often corresponded to the earth channel and water categories. When estimating the roughness of the riverbed, they were assigned the earth channel category. Ground truth segments were manually annotated by the authors directly on the photos and constituted reference material for analyses. The analysis of the photos was limited only to areas where water could potentially appear and where roughness estimation makes sense. They are marked in the photos as a white outline. These boundaries were determined manually by the authors after the photo segmentation process.

The image segmentation results were assessed using a confusion matrix, comparing actual (ground truth) segments to prediction settings [25,26]. Intersection over Union (*IoU*) was calculated from confusion matrix values to evaluate the SAM's performance [27] using True Positive (*TP*), False Negative (*FN*) and False Positive (*FP*) values.

$$IoU = \frac{TP}{TP + FN + FP} \quad (2)$$

Since the SAM is not a classic sematic segmentation model, the effect of segmentation are masks, which are assigned to appropriate categories in our method. Therefore, since the assignment to categories is manual, and the shapes of the masks themselves reproduce the shapes of objects very well, a False Positive does not occur.

### 3. Results and Discussion

The effectiveness of the segmentation algorithm of the two SAM versions on images of a mountain streambed is the main effect of the presented analysis. The results in Table 3 present two basic descriptive statistics of Intersection over Union (*IoU*). The average *IoU* value shows the averaged result, where the value of 0 can be interpreted as the worst possible result, and 1 as the best possible result to be obtained.

**Table 3.** Intersection over Union (*IoU*) mean and standard deviation for two selected SAM versions.

Category	SAM Online		SAM COLAB	
	<i>IoU</i> Mean	<i>IoU</i> Std.	<i>IoU</i> Mean	<i>IoU</i> Std.
Stones	0.68	0.14	0.61	0.06
Earth channel	0.54	0.04	0.57	0.04
Grass	0.55	0.38	0.17	0.17
Shrubs/trees	0.82	0.37	0.66	0.38
Water	0.49	0.48	0.01	0.02

The *IoU* standard deviation is a measure of model stability. It is clearly visible that, with the exception of the segmentation of the water and grass categories, the remaining results are similar for the two SAM launch modes used.

The best segmentation results of both models were obtained for the shrubs/trees category. However, this is also the category with the greatest variability of results. The most

unstable results were obtained when estimating the extent of floods (water category), where the online SAM model achieved an average *IoU* of 0.49, while SAM Colab practically did not recognize this category, with *IoU* practically at the minimum level. Similar results were obtained for the stones category, but in this case both models were very stable, achieving an *IoU* standard deviation in the range of 0.06–0.14. This is understandable because the SAM is better suited for segmenting specific objects, rather than larger areas in an image with a complex visual structure.

In the task of estimating riverbed roughness, SAM online performed well, considering the complexity of the images used. SAM Colab performed slightly worse, especially for the grass category. In the task of estimating the flood extent, SAM online performed well, obtaining an *IoU* mean of 0.49, while SAM Colab practically did not segment this category. It should be noted that only some of the photos used had a clearly visible water table, so this was an extremely difficult task.

Some regularities can be noticed in the image segmentation results presented in Table 3. The best results expressed by the Intersection over Union measure were obtained for categories that can be classified as physical objects. In this case, these are stones with an average *IoU* in both methods at the level of 0.61–0.68, but they are characterized by a very low standard deviation of 0.06–0.14. Even smaller variances with slightly worse results were obtained for the earth channel. In the case of segments covering a larger area (grass, shrubs/trees), significantly better identification is achieved using SAM online. This is especially visible in Figure 8, in the photographs from 28 October 2023 and from 14 March 2012, in terms of identifying areas covered with grass and shrubs.

In general, grass constitutes the smallest share of the area and is segmented well by SAM online, but much worse by SAM Colab. This can be seen in the images from 22 October 2011 and 28 October 2023 (Figure 8). Large stones pose the least problem to the segmentation model and are probably best identified in images. This can be explained by the fact that the SAM is designed to segment objects rather than uniform areas. Vegetation, if present in the image, is recognized well, probably due to a significantly different spectral signature than the background.

Detailed quantitative segmentation results for SAM online and SAM Colab are presented in Tables 4 and 5, respectively. The *IoU* = 1 value means extreme cases of identification: either the model did not detect areas in a given category because they did not appear in the photo or 100% of them were identified. This situation applies primarily to shrubs and trees.

**Table 4.** Intersection over Union (*IoU*) for SAM online.

Category	21 April 2010	27 May 2011	22 October 2011	14 March 2012	24 October 2015	28 May 2023	28 October 2023
Stones	0.70	0.77	0.83	0.76	0.45	0.52	0.69
Earth channel	0.52	0.53	0.53	0.51	0.61	0.56	0.51
Grass	0.61	0.09	0.71	1.00	0.18	0.23	1.00
Shrubs/trees	1.00	1.00	0.00	1.00	0.72	1.00	1.00

**Table 5.** Intersection over Union (*IoU*) for SAM Colab.

Category	21 April 2010	27 May 2011	22 October 2011	14 March 2012	24 October 2015	28 May 2023	28 October 2023
Stones	0.61	0.67	0.64	0.60	0.56	0.53	0.70
Earth channel	0.53	0.54	0.56	0.54	0.65	0.56	0.60
Grass	0.17	0.27	0.11	0.12	0.00	0.49	0.05
Shrubs/trees	1.00	1.00	0.53	0.00	0.42	1.00	0.64

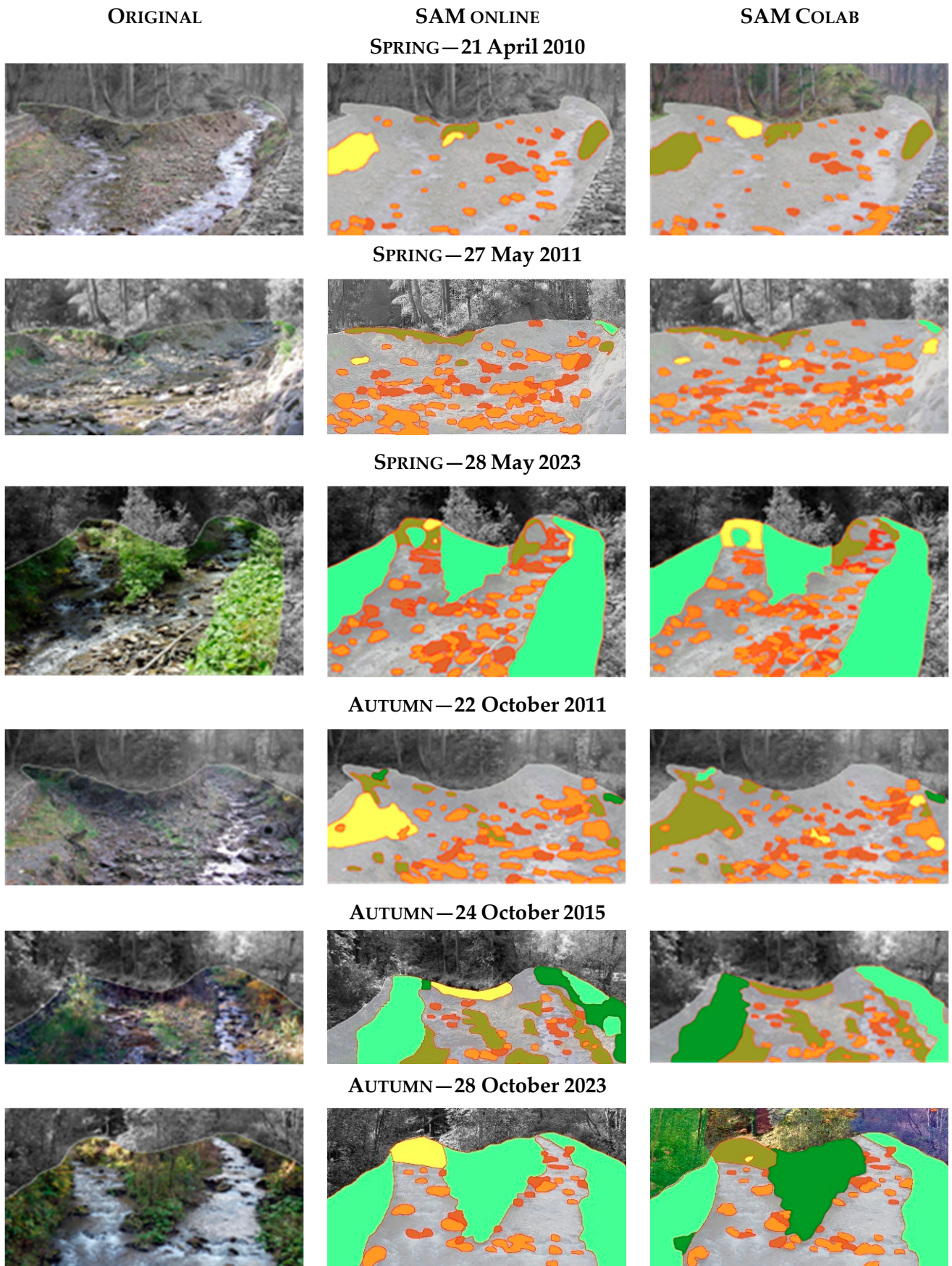
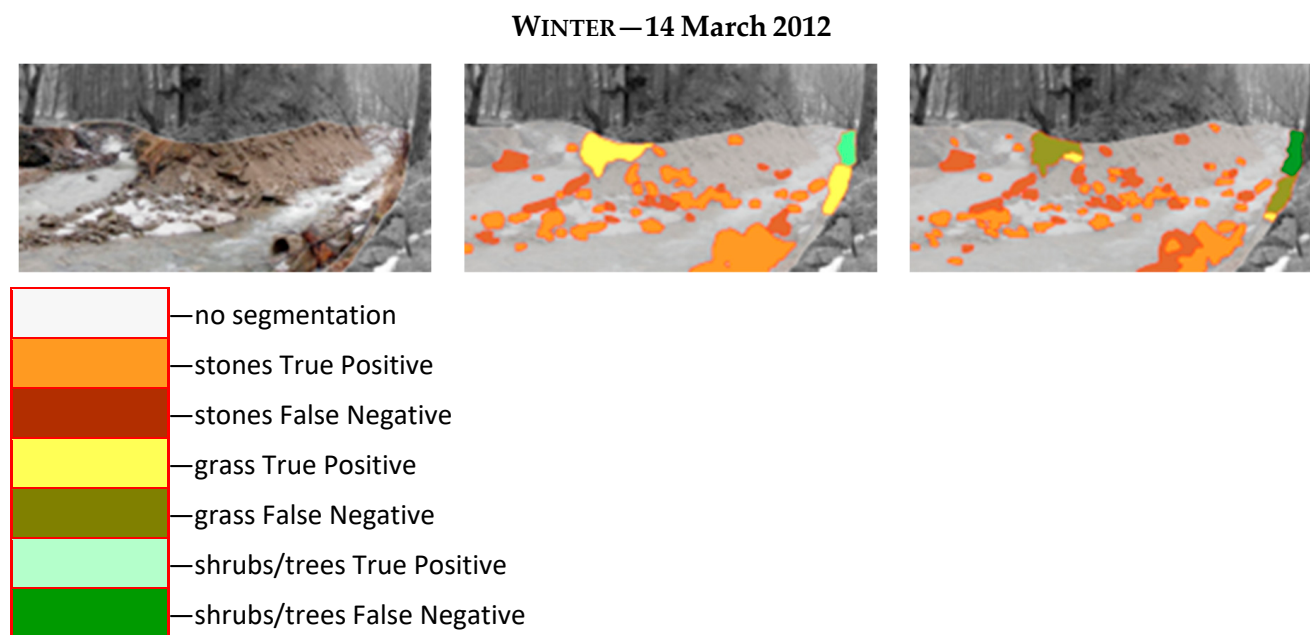


Figure 8. Cont.



**Figure 8.** Image segmentation in online automatic mode (SAM online) and in Jupyter notebook on Google Colaboratory (SAM Colab). The white outline marks the user-defined calculation area in which water may appear.

Both versions of the SAM model only perform segmentation occasionally ( $IoU = 0$ ). For SAM online, this applies to the image from 22 October 2011 for shrubs/trees (Table 4). For SAM Colab, such a situation occurred on 24 October 2015 for grass and on 14 March 2012 for shrubs/trees (Table 5). It is for the vegetation-related categories that  $IoU$  takes on its most extreme values, which is most visible for SAM online at shrubs/trees (Table 4). This may be related to the fact that there is relatively little vegetation in the area of the streambed, so the results obtained may be extremely different.

The worst segmentation results were obtained for grass with SAM Colab at a level not exceeding  $IoU = 0.5$ . This is understandable because the complex texture of low vegetation can be difficult to identify as an object.

Based on the image segmentation results, mean Manning's roughness coefficients were estimated by sections in cross-section A-A (Table 6). The obtained values were used to determine the average roughness coefficient for the entire riverbed cross-section using the weighted average method. Manning's roughness coefficient can be used in Manning's formula along with cross-sectional geometry and channel slope to estimate the flow in a stream. Changes in the roughness coefficient value can be noticed, especially in Sections 1, 3 and 5 in Table 6, where lush vegetation occurs especially in summer. The roughness coefficient is closely related to the growing season, as shown in Figure 4 and Tables 6 and 7. The obtained values of the roughness index  $R_c$  suggest a slightly different division into seasons than the division into seasons adopted in Table 7.

The end of May (28 May 2023) should be interpreted as a period of intense vegetation (summer, autumn) and the vegetation shown in the photo 22 October 2011 is more consistent with the winter season. However, it is impossible to generalize by introducing a strict division into growing seasons, because each year the seasons may start or end at different times. Therefore, the analysis of the streambed based on SAM segmentation makes it possible to determine more actual parameters related to hydraulic resistance. It is also worth noting that the range of changes in the roughness coefficient for the analyzed section of the streambed is large (in the range of 0.027–0.059) and may significantly affect the flow conditions.

The second aim of the analysis was to assess the effectiveness of the SAM segmentation results for estimating flood extent. Detailed effects are presented in the segmentation results

of the main stream (Wielka Puszczka on the left) and its tributary (Roztoka stream on the right) (Figure 9). In this case, the focus was only on the water category.

**Table 6.** Streambed roughness coefficients divided into sections of the wetted perimeter.

Section Number		1	2	3	4	5	Weighted Average
Wetted perimeter [m]		6.75	4.13	2.60	3.57	6.90	
21 April 2010	Roughness coefficient	0.025	0.028	0.027	0.025	0.027	0.026
Category	Stones	0%	19%	14%	2%	0%	
	Earth channel	98%	81%	86%	98%	60%	
	Grass	2%	0%	0%	0%	40%	
	Shrubs/trees	0%	0%	0%	0%	0%	
22 November 2011	Roughness coefficient	0.032	0.030	0.030	0.028	0.029	0.030
Category	Stones	12%	34%	30%	20%	6%	
	Earth channel	71%	64%	63%	80%	29%	
	Grass	12%	2%	7%	0%	65%	
	Shrubs/trees	6%	0%	0%	0%	0%	
28 May 2023	Roughness coefficient	0.100	0.034	0.078	0.029	0.097	0.075
Category	Stones	0%	27%	3%	25%	0%	
	Earth channel	0%	67%	27%	75%	3%	
	Grass	0%	0%	0%	0%	0%	
	Shrubs/trees	100%	6%	70%	0%	97%	

**Table 7.** Streambed roughness index ( $R_c$ ) divided into seasons.

Season	Data	SAM Online	SAM Colab
Spring	21 April 2010	0.027	0.027
	25 May 2011	0.029	0.029
	28 May 2023	0.059	0.058
Autumn	24 October 2015	0.050	0.050
	28 October 2023	0.059	0.059
	22 October 2011	0.029	0.029
Winter	14 March 2012	0.029	0.029

A fragment of the streambed that has been subjected to vision analysis poses a great challenge to segmentation algorithms. In the image from 27 May 2011 (Figure 9), it is difficult even for humans to recognize fragments with water because the photo was taken at an extremely low water level. The image from 24 October 2015 is equally difficult to segment. In this case, one of the streams was correctly identified, while the other one was not identified at all. In images where water is an important part (21 April 2010, 28 October 2023, 14 March 2012), SAM online had no problems with good segmentation of this category, although SAM Colab did not cope with this task. Analyzing the segmentation in terms of flood extent, it can be seen that only in one out of four cases for higher water levels did SAM online fail to detect the water table (Table 8). In the remaining cases, the  $IoU$  results were no less than 0.94, which can be considered an excellent result.

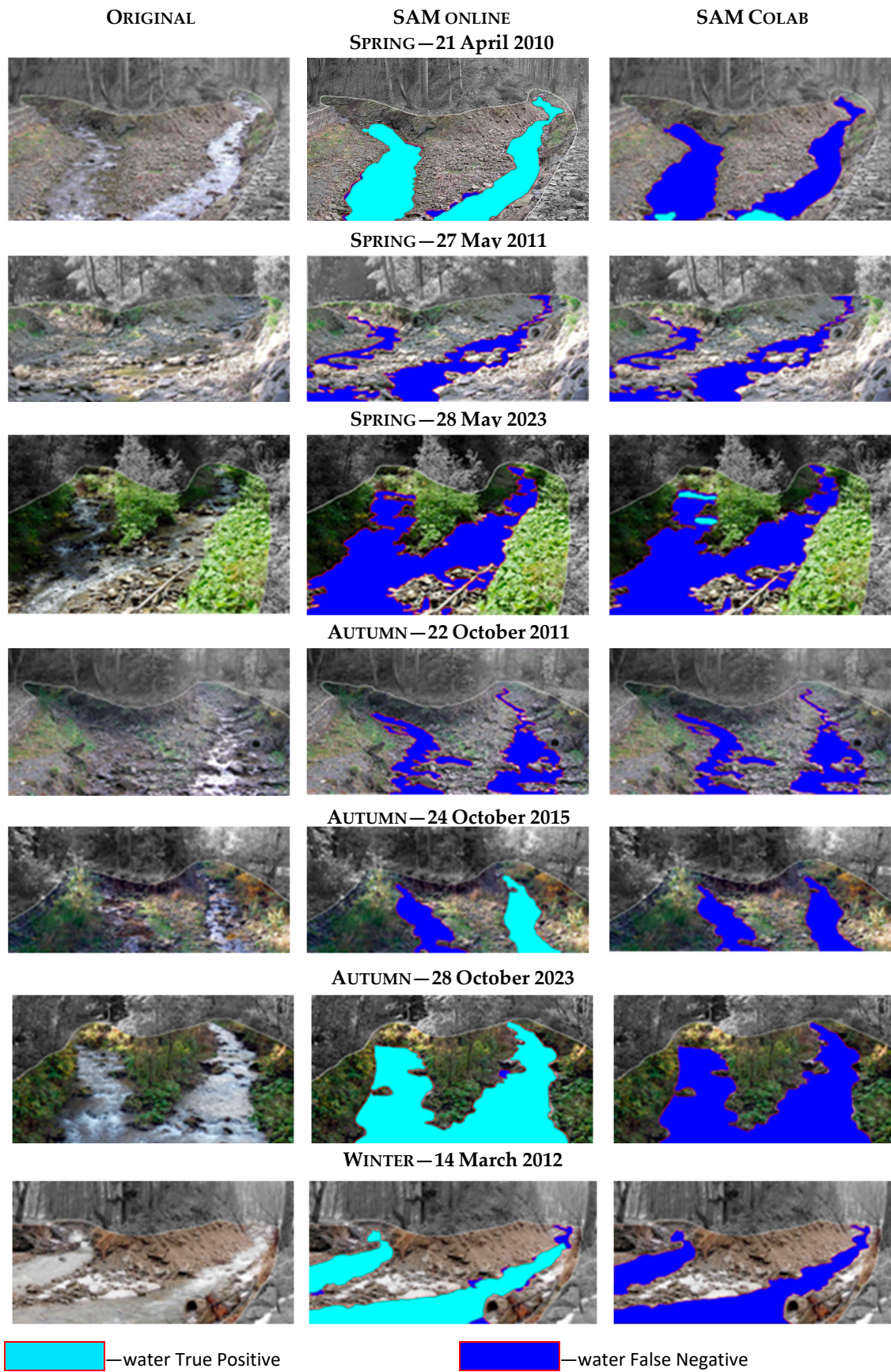


**Figure 9.** The result of water segmentation in a mountain streambed. The white outline marks the user-defined calculation area in which water may appear.

**Table 8.** Intersection over Union (*IoU*) for water category, (\*)—water table above low levels.

Model	21 April 2010 *	27 May 2011	22 October 2011	14 March 2012 *	24 October 2015	28 May 2023 *	28 October 2023 *
SAM online	0.97	0.00	0.00	0.94	0.53	0.00	0.96
SAM Colab	0.06	0.00	0.00	0.00	0.00	0.02	0.00

The very large variance of the SAM online results is also significant, as only in one case (24 October 2015) was the *IoU* not close to 0 or 1. The SAM Colab segmentation results were extremely poor. In many images, water appears only between the stones.

For the initial estimation of Manning's roughness coefficient  $n$  in ungauged catchments, empirical formulas employing pebble count and field survey data can be applied [28]. These tasks can be automated using the presented method for predefined gravel riverbed material (d50, d65, d75, d84 and d94). Changes in fluvial forms and cover within the riverbed can also be examined using aerial photos or photos from unmanned aerial vehicles [29]. For some locations, these methods may prove to be the most economically effective. In our case, due to the dense tree crowns along the streams, such a solution could not be used. Seasonal changes in flows are visible in many places in the Carpathians [30]. A detailed analysis of the impact of seasonal vegetation changes on the roughness coefficient estimation can be found in [31]. Seasonal changes in flows are directly related to climate change in the area [32] and have a direct impact on flood hazard mapping [33]. According to hydrological and climatological research conducted in the Carpathian area, even greater variability in droughts and floods can be expected in the future [34–37]. As a result, there is a need for tools that can automatically track these changes.

The analyzed area is characterized by very fast and short-lasting floods. For this reason, very few photos are available from the flood period itself. The available photographic documentation from the studied stream cross-section did not contain a sufficient number of images from the flood; therefore, three additional photos were analyzed (Figure 10).

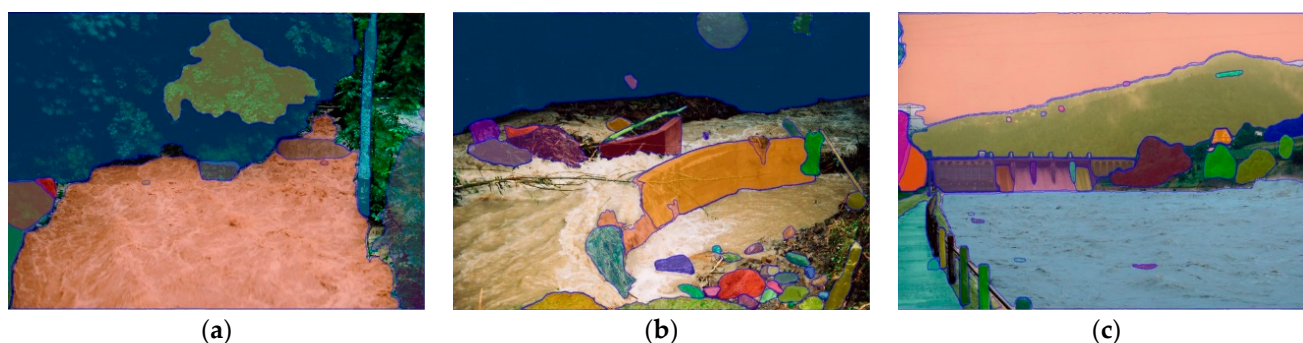


**Figure 10.** The SAM online segmentation result of flood water extent; (a,b) flood in 1997 on the Roztoka stream; (c) flood in 1997 on the Soła River.

An additional difficulty may be the lighting conditions, where the shadows of trees mix with stones and low vegetation. The SAM was created for object recognition, but such a complex structure as a mountain stream slightly filled with water seems too difficult a challenge. In the case of uniformly illuminated water surfaces (Figure 10a,c), SAM online is easily able to segment the flood water table. The remaining image elements are segmented equally well. The third photo, taken during the flood at night (Figure 10b), segments all objects very well, except for the turbulent and unevenly lit stream. However, it can be assumed that in this case the flood extent corresponds to the entire remaining area, so it is easy to identify and further process. The quality of segmentation depends not only on the texture of the object, but also on its lighting.

The SAM online provides automatic image segmentation without the ability to manage model parameters, which poses some limitations, but the quality of the results obtained is

satisfactory. The average *IoU* ranges from 0.55 for grass to 0.82 for shrubs/trees. However, it is worth noting the high standard deviations of the results. The high variability of the SAM results, expressed here by high *IoU* standard deviations, was also observed by other authors [15]. According to Mazurowski et al. [16], the SAM's performance based on single prompts highly varies depending on the dataset and the task, from *IoU* = 0.11 for a spine MRI (Magnetic Resonance Image) to *IoU* = 0.86 for a hip X-ray. In our study, most categories are either segmented well (very well) or not segmented at all. This is clearly visible in the online SAM results for the shrubs, trees and water categories, where *IoU* equal to 0 or close to 1 dominates. As reported by Huang et al. [38], the SAM showed remarkable performance in some specific objects but was unstable, imperfect or even totally failed in other situations. As this study showed, with the appropriate selection of images, you can quickly obtain an estimate of the flood extent at the level of at least *IoU* = 0.94. For a similar task, Tedesco and Radzikowski [5] reported *IoU* of 0.84–0.98 using deep convolutional neural networks (D-CNNs). In all analyzed cases, the quality of images and uniform lighting are of great importance. The SAM, which is a zero-shot model that does not require training, performs segmentation very well. Most importantly, it is available for free and does not require knowledge of machine learning for practical use.

#### 4. Conclusions

The Segment Anything Model (SAM) presented in this paper is a new tool with a potentially very wide range of applicability, also in hydrology. Unlike dedicated models, it is trained on a large and diverse datasets. The roughness coefficient is not easy to determine and is varying constantly both in space along the length of the streams and in time in subsequent growing seasons. It is influenced by the meandering character of the river, the bed material and the average grain size, the channel bed forms, the channel obstructions, the geometry changes between sections and the vegetation in the channel [31]. In the presented analysis, we showed how it can be estimated for a specific cross-section and as an average index value for a fragment of a watercourse. The advantage of the proposed method is its simplicity, low cost and scalability. The analysis presented for one cross-section can be repeated for any number of cross-sections in different seasons of the year based only on digital photographs.

Two versions of the SAM were tested in the task of segmenting images of a mountain streambed in order to estimate the roughness coefficient. In a similar way, the SAM was used to estimate the extent of floods. To the best of our knowledge, this is the first described application of the SAM for estimating riverbed roughness and one of the first for estimating flood extent.

The SAM Colab provides opportunities to optimize model parameters, but this requires experience in machine learning. With the default parameters, the segmentation results are rather unsatisfactory. Similarly, He et al. [15] observed that the SAM, when directly applied to medical images without re-training or fine-tuning, is not yet as accurate as algorithms specifically designed for medical image segmentation tasks. To better adapt the SAM to dedicated tasks in the area of hydrological applications, training and tuning of the SAM Colab model would be required.

**Author Contributions:** Conceptualization, B.B., M.B. and R.S.; methodology, B.B., M.B. and R.S.; software, B.B., M.B. and R.S.; validation, B.B., M.B. and R.S.; formal analysis, B.B., M.B. and R.S.; investigation, B.B., M.B. and R.S.; resources, B.B., M.B. and R.S.; data curation, B.B., M.B. and R.S.; writing—original draft preparation, B.B., M.B. and R.S.; writing—review and editing, B.B., M.B. and R.S.; visualization, B.B., M.B. and R.S. All authors have read and agreed to the published version of the manuscript.

**Funding:** This research received no external funding.

**Data Availability Statement:** The photographs analyzed in this article are available on the website: [https://holmes.iigw.pl/~mbodzion/zaklad/wielka\\_puszcza/](https://holmes.iigw.pl/~mbodzion/zaklad/wielka_puszcza/) (accessed on 20 January 2024).

**Conflicts of Interest:** The authors declare no conflict of interest.

## References

- Bentivoglio, R.; Isufi, E.; Jonkman, S.N.; Taormina, R. Deep Learning Methods for Flood Mapping: A Review of Existing Applications and Future Research Directions. *Hydrol. Earth Syst. Sci.* **2021**, *26*, 4345–4378. [[CrossRef](#)]
- Muhadi, N.A.; Abdullah, A.F.; Bejo, S.K.; Mahadi, M.R.; Mijic, A. Deep Learning Semantic Segmentation for Water Level Estimation Using Surveillance Camera. *Appl. Sci.* **2021**, *11*, 9691. [[CrossRef](#)]
- Lo, S.-W.; Wu, J.-H.; Lin, F.-P.; Hsu, C.-H. Visual Sensing for Urban Flood Monitoring. *Sensors* **2015**, *15*, 20006–20029. [[CrossRef](#)]
- Lopez-Fuentes, L.; Rossi, C.; Skinnemoen, H. River segmentation for flood monitoring. In Proceedings of the 2017 IEEE International Conference on Big Data (Big Data), Boston, MA, USA, 11–14 December 2017; pp. 3746–3749. [[CrossRef](#)]
- Tedesco, M.; Radzikowski, J. Assessment of a Machine Learning Algorithm Using Web Images for Flood Detection and Water Level Estimates. *Geohazards* **2023**, *4*, 437–452. [[CrossRef](#)]
- Pally, R.; Samadi, S. Application of image processing and convolutional neural networks for flood image classification and semantic segmentation. *Environ. Model. Softw.* **2022**, *148*, 105285. [[CrossRef](#)]
- Erfani, S.M.H.; Wu, Z.; Wu, X.; Wang, S.; Goharian, E. ATLANTIS: A benchmark for semantic segmentation of waterbody images. *Environ. Model. Softw.* **2022**, *149*, 105333. [[CrossRef](#)]
- Shen, C.; Chen, X.; Laloy, E. Broadening the use of machine learning in hydrology. *Front. Water* **2021**, *3*, 681023. [[CrossRef](#)]
- Djajadi, R. Comparative study of equivalent manning roughness coefficient for channel with composite roughness. *Civ. Eng. Dimens.* **2009**, *11*, 113–118. [[CrossRef](#)]
- Fisher, K.R.; Dawson, F. *Reducing Uncertainty in River Flood Conveyance: Roughness Review*; Report Number: Project W5A-057—DEFRA; Flood Management Division & Science Directorate, & Environment Agency: Lincoln, UK, 2003; 204p.
- Nagy, B. A creek's hydrological model's generates in HEC-RAS. In Proceedings of the Student V4 Geoscience Conference and Scientific Meeting GISÁČEK, Ostrava, Czech Republic, 22 March 2017; Technical University of Ostrava: Ostrava, Czech Republic, 2017.
- Bhola, P.K.; Nair, B.B.; Leandro, J.; Rao, S.N.; Disse, M. Flood inundation forecasts using validation data generated with the assistance of computer vision. *J. Hydroinform.* **2018**, *21*, 240–256. [[CrossRef](#)]
- Carion, N.; Massa, F.; Synnaeve, G.; Usunier, N.; Kirillov, A.; Zagoruyko, S. End-to-end object detection with transformers. In *European Conference on Computer Vision*; Springer International Publishing: Cham, Switzerland, 2020; pp. 213–229. [[CrossRef](#)]
- Kirillov, A.; Mintun, E.; Ravi, N.; Mao, H.; Rolland, C.; Gustafson, L.; Xiao, T.; Whitehead, S.; Berg, A.C.; Lo, W.; et al. Segment Anything. *arXiv* **2023**, arXiv:2304.02643. [[CrossRef](#)]
- He, S.; Bao, R.; Li, J.; Grant, P.E.; Ou, Y. Accuracy of segment-anything model (sam) in medical image segmentation tasks. *arXiv* **2023**, arXiv:2304.09324. [[CrossRef](#)]
- Mazurowski, M.A.; Dong, H.; Gu, H.; Yang, J.; Konz, N.; Zhang, Y. Segment anything model for medical image analysis: An experimental study. *Med. Image Anal.* **2023**, *89*, 102918. [[CrossRef](#)] [[PubMed](#)]
- Li, Y.; Wang, D.; Yuan, C.; Li, H.; Hu, J. Enhancing Agricultural Image Segmentation with an Agricultural Segment Anything Model Adapter. *Sensors* **2023**, *23*, 7884. [[CrossRef](#)] [[PubMed](#)]
- Luo, X.; Walther, P.; Mansour, W.; Teuscher, B.; Zollner, J.M.; Li, H.; Werner, M. Exploring GeoAI Methods for Supraglacial Lake Mapping on Greenland Ice Sheet. In Proceedings of the SIGSPATIAL '23: 31st ACM International Conference on Advances in Geographic Information Systems, Hamburg, Germany, 13–16 November 2023. [[CrossRef](#)]
- Li, W.; Lee, H.; Wang, S.; Hsu, C.Y.; Arundel, S.T. Assessment of a new GeoAI foundation model for flood inundation mapping. In Proceedings of the 6th ACM SIGSPATIAL International Workshop on AI for Geographic Knowledge Discovery, Hamburg, Germany, 13 November 2023; pp. 102–109. [[CrossRef](#)]
- Ren, S.; Luzzi, F.; Lahrichi, S.; Kassaw, K.; Collins, L.M.; Bradbury, K.; Malof, J.M. Segment anything, from space? *arXiv* **2023**, arXiv:2304.13000. [[CrossRef](#)]
- Boulomytis, V.T.G.; Zuffo, A.C.; Filho, J.G.D.; Alam Imteaz, M. Estimation and calibration of Manning's roughness coefficients for ungauged watersheds on coastal floodplains. *Int. J. River Basin Manag.* **2017**, *15*, 199–206. [[CrossRef](#)]
- Abbas, M.R.; Hason, M.M.; Bin Ahmad, B.; Abbas, T.R. Surface roughness distribution map for Iraq using satellite data and GIS techniques. *Arab. J. Geosci.* **2020**, *13*, 839. [[CrossRef](#)]
- Hossain, A.K.M.A.; Jia, Y.; Chao, X. Estimation of Manning's roughness coefficient distribution for hydrodynamic model using remotely sensed land cover features. In Proceedings of the 2009 17th International Conference on Geoinformatics, Fairfax, VA, USA, 12–14 August 2009; pp. 1–4. [[CrossRef](#)]
- Chow, V.T. *Open Channel Hydraulics*; McGraw-Hill Book Co.: New York, NY, USA, 1959.
- Reinke, A.; Tizabi, M.D.; Sudre, C.H.; Eisenmann, M.; Radsch, T.; Baumgartner, M.; Maier-Hein, L. Common limitations of image processing metrics: A picture story. *arXiv* **2021**, arXiv:2104.05642. [[CrossRef](#)]
- Wang, Z.; Wang, E.; Zhu, Y. Image segmentation evaluation: A survey of methods. *Artif. Intell. Rev.* **2020**, *53*, 5637–5674. [[CrossRef](#)]
- Hernández, D.; Cecilia, J.M.; Cano, J.-C.; Calafate, C.T. Flood detection using real-time image segmentation from unmanned aerial vehicles on edge-computing platform. *Remote Sens.* **2022**, *14*, 223. [[CrossRef](#)]
- Papaioannou, G.; Vasiliades, L.; Loukas, A.; Aronica, G.T. Probabilistic flood inundation mapping at ungauged streams due to roughness coefficient uncertainty in hydraulic modelling. *Adv. Geosci.* **2017**, *44*, 23–34. [[CrossRef](#)]

29. Korpak, J. Assessment of changes in channel morphology in a mountain river regulated using grade control structures. *J. Ecol. Eng.* **2020**, *21*, 163–176. [[CrossRef](#)]
30. Tomalski, P.; Tomaszewski, E.; Wrzesiński, D.; Sobkowiak, L. Relationships of hydrological seasons in rivers and groundwaters in selected catchments in Poland. *Water* **2021**, *13*, 250. [[CrossRef](#)]
31. De Doncker, L.; Troch, P.; Verhoeven, R.; Bal, K.; Meire, P.; Quintelier, J. Determination of the Manning roughness coefficient influenced by vegetation in the river Aa and Biebrza river. *Environ. Fluid Mech.* **2009**, *9*, 549–567. [[CrossRef](#)]
32. Wrzesiński, D.; Marsz, A.A.; Sobkowiak, L.; Styszyńska, A. Response of low flows of polish rivers to climate change in 1987–1989. *Water* **2022**, *14*, 2780. [[CrossRef](#)]
33. Gądek, W.; Baziak, B.; Tokarczyk, T.; Szalińska, W. A Novel Method of Design Flood Hydrographs Estimation for Flood Hazard Mapping. *Water* **2022**, *14*, 1856. [[CrossRef](#)]
34. Baran-Gurgul, K. The Risk of Extreme Streamflow Drought in the Polish Carpathians—A Two-Dimensional Approach. *Int. J. Environ. Res. Public Health* **2022**, *19*, 14095. [[CrossRef](#)]
35. Bogdanowicz, E.; Karamuz, E.; Romanowicz, R.J. Temporal Changes in Flow Regime along the River Vistula. *Water* **2021**, *13*, 2840. [[CrossRef](#)]
36. Cebulska, M.; Kholiavchuk, D. Variability of meteorological droughts in the polish and the Ukrainian Carpathians, 1984–2015. *Meteorol. Atmos. Phys.* **2022**, *134*, 17. [[CrossRef](#)]
37. Twaróg, B. Characteristics of multi-annual variation of precipitation in areas particularly exposed to extreme phenomena. Part 1. The upper Vistula river basin. *E3S Web Conf.* **2018**, *49*, 00121. [[CrossRef](#)]
38. Huang, Y.; Yang, X.; Liu, L.; Zhou, H.; Chang, A.; Zhou, X.; Chen, R.; Yu, J.; Chen, J.; Chen, C.; et al. Segment anything model for medical images? *Med. Image Anal.* **2023**, *92*, 103061. [[CrossRef](#)]

**Disclaimer/Publisher’s Note:** The statements, opinions and data contained in all publications are solely those of the individual author(s) and contributor(s) and not of MDPI and/or the editor(s). MDPI and/or the editor(s) disclaim responsibility for any injury to people or property resulting from any ideas, methods, instructions or products referred to in the content.